VOL. 5, NO. 3, MARCH 2010 ISSN 1819-6608
ARPN Journal of Engineering and Applied Sciences


www.arpnjournals.com

EXPLICIT DYNAMIC SIMULATION OF DROP-WEIGHT LOW VELOCITY IMPACT ON CARBON FIBROUS COMPOSITE PANELS

Umar Farooq and Karl Gregory
School of Built Environment and Department of Engineering, University of Bolton, United Kingdom
E-Mail: uf1res@bolton.ac.uk; k.r.gregory@bolton.ac.uk

ABSTRACT

Finite element computational model was developed to simulate impact behaviour and predict the failure response of carbon fibrous composite panels subjected to low velocity drop-weight impact on the partitioned area where an impactor of flat-nosed tip hits the target. Critical damage regions under impactors' tips are very complicated phenomenon to study since internal load re-distributes after impact and damage accumulates in through-the-thickness plies. Transformation of mathematical formulations into numerical model and writing modular code also need extensive efforts and time. However, efficient way of solving the problems using commercial software generated simulations. For this work, commercially available software ABAQUS^{TM} was selected, which incorporates shell elements and stacks of plies. The user Table option of the software provides an extended amount of input data without having to re-link the code that could be utilised for various load cases. Model developing and simulation techniques associated with the software usage are presented herein. The developed models are capable to simulate impact phenomena of various drop weights for parametric studies. The methodology applied consists of computing in-plane stresses from the model and using Trapezium rule to calculate transverse shear stresses from the standard equilibrium equations. The method is simple and efficient to predict equivalent 3-D transverse shear stresses from a 2-D model. These predicted and calculated stresses were used in failure theories to predict possible failure modes. Some of the results from failure threshold loads were selected and included in the form of tables, contour plots and graphs.

Keywords: model, low velocity impact, fibre reinforced composites, transverse shear stresses, drop-weights, finite element simulation.

INTRODUCTION

Advanced fibrous composites are being used in many advanced structural applications: aeronautical, aerospace, naval and other industries mainly because of their attractive properties compared to isotropic materials such as higher stiffness/weight, higher strength, higher damping and good properties related to thermal or acoustic isolation, among others. Many of these structures are situated where their locations are susceptible to foreign object impacts and out-of-plane loadings which cause invisible extensive damage. The damage can significantly reduce the load bearing capability or cause catastrophic failures. Thus there exists the need to investigate the incurred damage to be able to improve damage tolerance and life expectancy of structures. Most of the available literature is experimental with little discussion on computational modeling of drop-weight impacts. Some of the relevant studies found in the existing literature are given below:

Dynamic large deflection response of composite laminates subjected to impact was studied by Chen in (Chen, 1985). Impact on laminated composites was investigated in (Abrate, 1991). A new approach toward understanding damage mechanisms and mechanics of laminated composites due to low velocity impact loading was developed by Chang in (Chang, 1991). A model for predicting damage in graphite/epoxy composites resulting from low-velocity point impact was developed by Choi in (Choi, 1992). Low-velocity impact response of composites considering higher-order shear deformation and large deflection was investigated by Choi in (Choi, 1994). Response and damage of composite laminates subjected to low-velocity impact was simulated by Cho in his PhD thesis (Choi, 1994). Estimation of damage area due to low-velocity impact in composite laminate was predicted by Hong in (Hong, 1994). The damage tolerance of GRP laminates under biaxial prestress was computed by Robb in (Robb, 1995). Pierson in (Pierson, 1995) determined analytical solution for low-velocity impact response of composites. Sekine in (Sekine, 1998) studied low-velocity impact response of composite plates. Failure analysis of laminated composite shell panels subjected low velocity impact was conducted in (Ganapathy, 1998). Mili, F., and Necib, B., in (Mili, 2001) reported impact behaviour of cross-ply composites under low velocities. Modelling of impacts on composite structures was investigated in (Abrate, 2001). Li. C.F., and Fukunaga, H., in (Li, 2002) estimated low-velocity impact damage of composites. Aslan Z., and Okutan, B., in (Aslan, 2003) studied the response of composites under low-velocity impact. The response of composites with pre-stress subject to low velocity impact damage was investigated in (Whittingham, 2004). James, R. A, in his PhD thesis (James, 2006) investigated impact damage resistance and damage tolerance of fibrous composites. Analysis of low-velocity impact on preloaded GFRP specimens with various impactor shapes was presented in (Mitrevski, 2006). Damage prediction in composite plates subjected to low velocity impact was made in (Tiberkak, 2008). A computational model was developed by Farooq in (Farooq, 2009) to simulate the un-partitioned drop-weight low velocity impact on fibrous composites.

Review of the relevant studies revealed that most of the research on the topic in the past has been

experimental focusing on developing phenomenological and semi-analytical models based on experimental observations. Therefore, a suitable computational model is essential to exploit the full benefits of the advanced composites. Hence, the problem was transformed into numerical model to simulate and obtain adequate, consistent and reliable results. Moreover, an incidental or drop tool may not always impact the panel on whole body but on a specific location. Therefore, impacted location was partitioned from rest of the body.

DEVELOPMENT OF SIMULATION MODEL

The drop-weight model to predict the composites behaviour was incorporated into ABAQUS™ program to simulate the model and generate the results. Circular discs of fibre reinforced composite plies of diameter 0.05 m with 0.00288 m thickness as shown in Figure-1 below were considered. Quasi-isotropic configurations of [45/0/-45/90] symmetric and non-symmetric plies were partitioned at the centre for 2.1 mm, 4.2 mm, and 6.3 mm. Each layer of elements through the thickness was treated as a single ply. Simulation for overall laminate stiffness of each ply in the model rotated to align the major ply mechanical properties with the principal fibre directions in the Table-2. Depicted ply configuration for 24-ply model can be seen from the Figure-5.

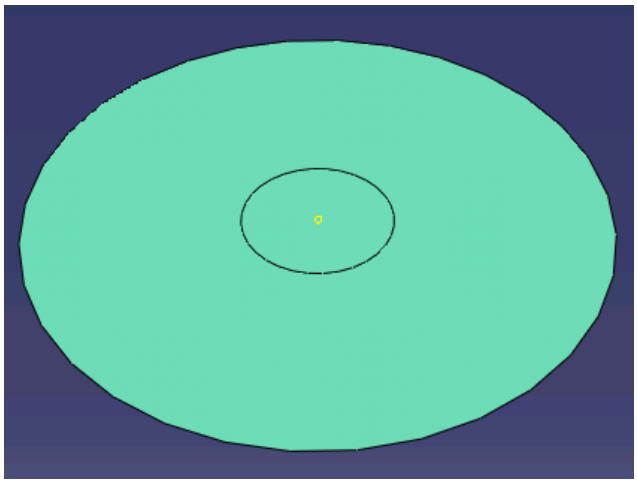

Figure-1. Schematic diagram of specimen.

Figure-2. Impactor used in the simulation.

Centrally located impactor of circular diameter 0.0063 m diameter and of length 0.002 m made up from aluminum as shown in Figure-2 was selected to impact the target as the drop-weight.

The circular disk and impactor were assembled, fully constrained as both axial and rotational restraints were applied to the edge boundaries, and loaded as shown in Figure-3 below.

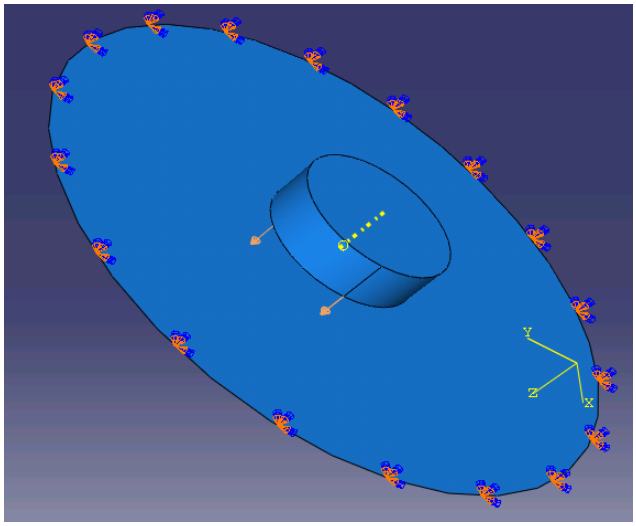

Figure-3. Model after applying load and boundary conditions.

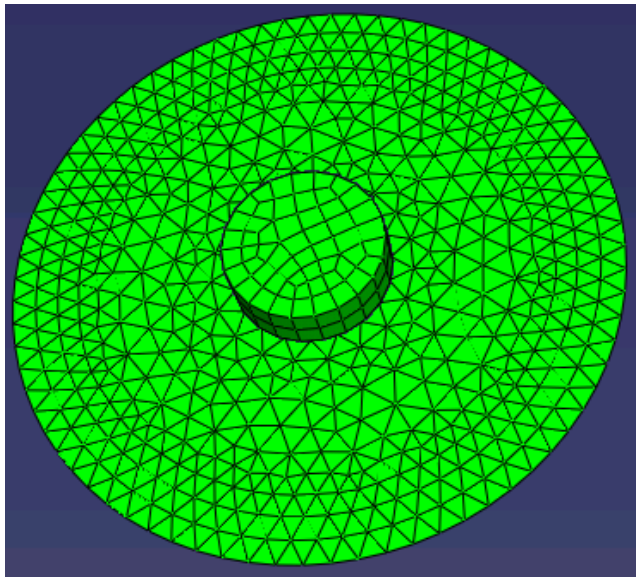

Figure-4. Meshed model.

Contacts and constraints of the parts were defined in the Interaction module. In the Mesh module meshing elements, family, and sizes were selected and meshed as shown below Figure-4. Meshes were generated from finite elements: (a) Shell element S3/S3R and S4/SC6R for specimen and (b) Solid element C3D8 for impactor.

Table-1. Material properties used in simulations.

Material properties	**Ultimate strengths** (MPa)
Elastic constants (GPa) $E_1 = 150$, $E_2 = E_3 = 15$; $G_{12} = 5.7$, $G_{13} = 5.7$, $G_{23} = 7.26$	$\left(\sigma_1^T\right)_{ult} = 1500$
	$\left(\sigma_1^C\right)_{ult} = 1500$
	$\left(\sigma_2^T\right)_{ult} = 40$
Poisson's ratios $\nu_{12} = 0.33$ $\nu_{23} = 0.03$ $\nu_{13} = 0.01$	$\left(\sigma_2^C\right)_{ult} = 20$
	$\left(\tau_{12}\right)_{ult} = \left(\tau_{12}\right)_{ult} = 53$

Properties were entered into the software through the following Edit Composite lay-up dialogue

Table-2. Dialog box to enter input data.

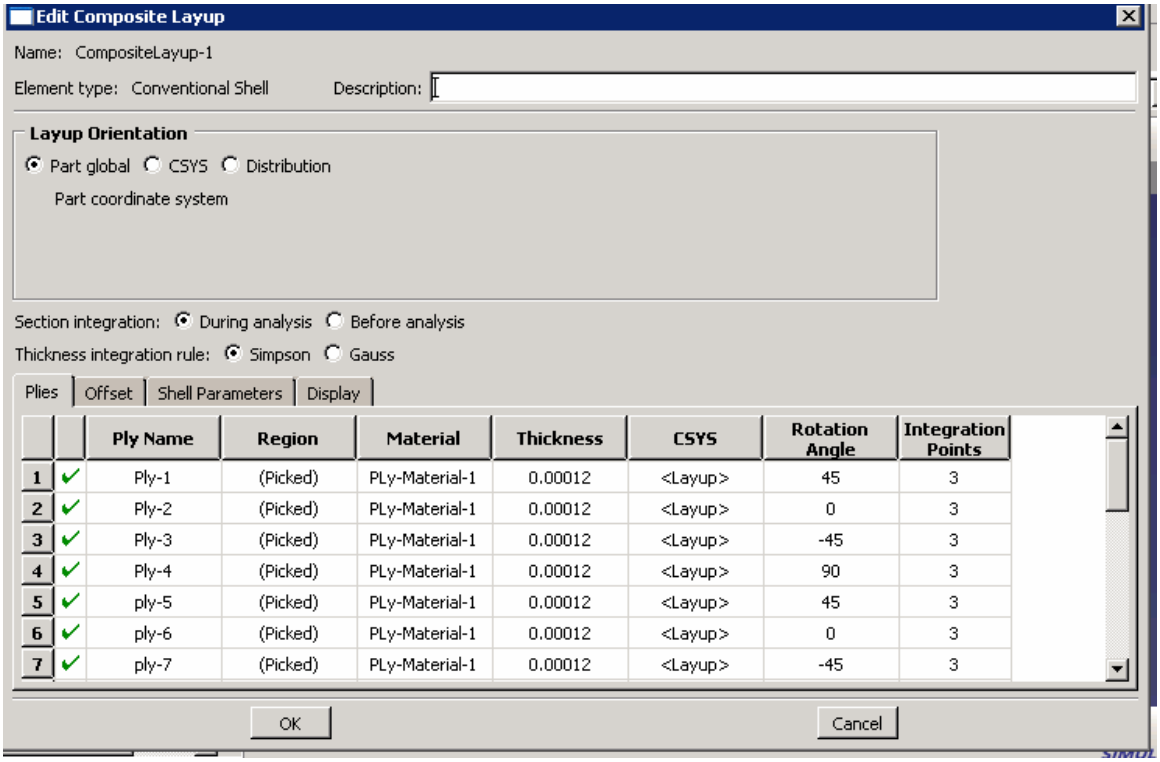

		Ply Name	Region	Material	Thickness	CSYS	Rotation Angle	Integration Points
1	✔	Ply-1	(Picked)	PLy-Material-1	0.00012	<Layup>	45	3
2	✔	Ply-2	(Picked)	PLy-Material-1	0.00012	<Layup>	0	3
3	✔	Ply-3	(Picked)	PLy-Material-1	0.00012	<Layup>	-45	3
4	✔	Ply-4	(Picked)	PLy-Material-1	0.00012	<Layup>	90	3
5	✔	ply-5	(Picked)	PLy-Material-1	0.00012	<Layup>	45	3
6	✔	ply-6	(Picked)	PLy-Material-1	0.00012	<Layup>	0	3
7	✔	ply-7	(Picked)	PLy-Material-1	0.00012	<Layup>	-45	3

The stacking sequences generated are shown in the following Figure-6, in order to verify the model specification and input data.

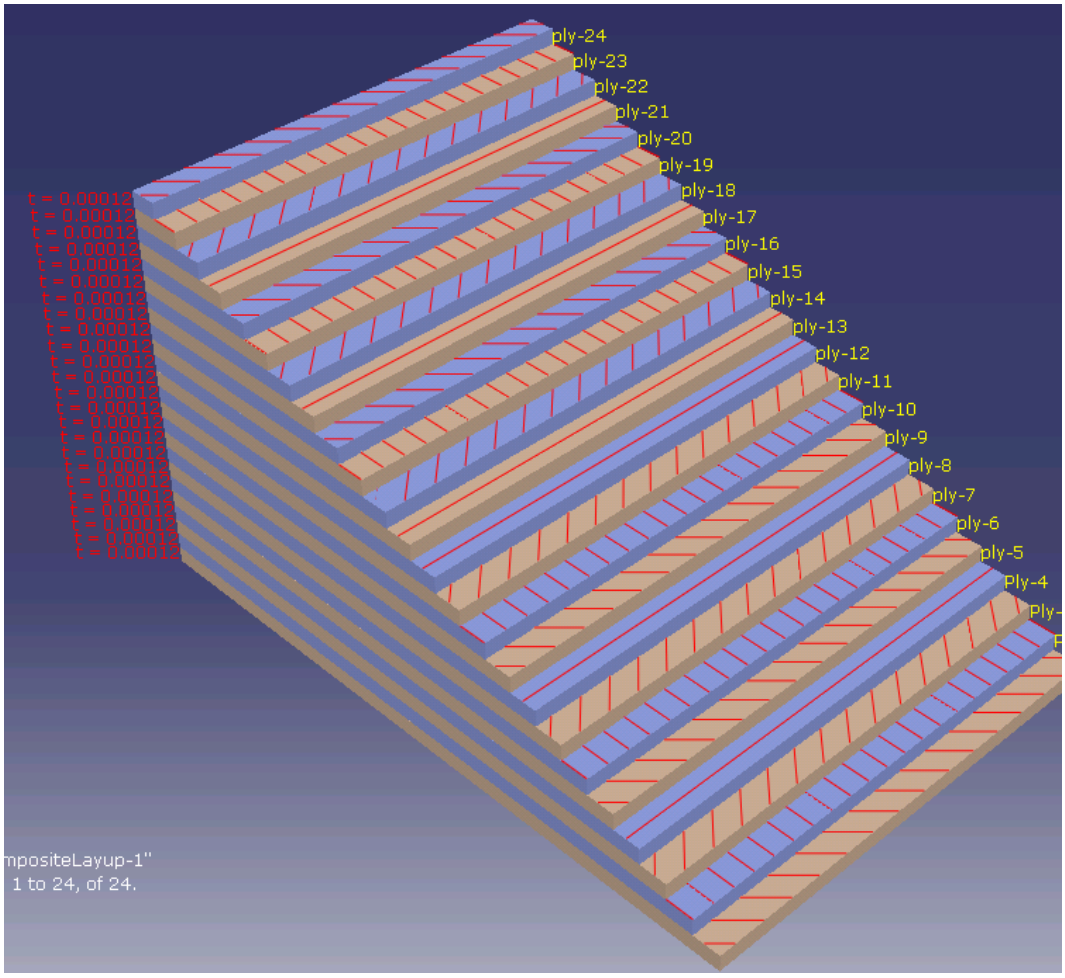

Figure-5. Stack of plies.

The drop-weight models were simulated for velocity (3 m/sec) and time duration 1.1 μs, Amplitudes of velocities shown in the Table-2 were used to impact the target.

Table-3. Time (s) and 5 amplitudes to multiply velocities (m/s).

Time (μs)	**Amplitudes** (non-dimensional)				
	1	2	3	4	5
	.05	.05	.02	.05	.05
0.0	.08	.05	.02	0.1	0.1
5.5	.15	.06	.03	0.2	0.1
11	0.3	0.1	.04	0.3	0.1
16.5	0.4	0.2	.05	0.4	0.1
22	0.5	0.3	0.1	0.5	0.2
27.5	0.6	0.4	0.2	0.6	0.2
33	0.7	0.5	0.3	0.7	0.2
38.5	0.8	0.6	0.4	0.8	0.3
44	0.9	0.8	0.5	0.9	0.8
49.5	1	0.9	0.6	1	0.9
55	0.9	1	0.7	0.9	1
60.5	0.8	0.9	0.8	0.8	0.9
66	0.6	0.8	0.9	0.7	0.8
7.15	0.5	0.7	1	0.6	0.3
77	0.4	0.6	0.9	0.5	0.3
8.25	0.3	0.5	0.8	0.4	0.2
88	0.3	0.4	0.7	0.4	0.2
93.5	0.2	0.2	0.6	0.3	0.2
99	0.2	0.3	0.5	0.3	0.2
105	0.2	0.3	0.4	0.3	0.2

Given the fixed ply thickness for the material results for stresses and strains were generated for various simulation models.

NUMERICAL RESULTS AND DISCUSSIONS

Computer generated results were presented in tabular, graphs and contour plot. These results provided information as a basis to build analysis for the composite panels subjected to impacts from various nose impactors. The design procedure illustrated can be very time consuming if all potential lay-ups, tests, and results are examined. From bulk of the results top most ply out of 24-ply model was selected for discussion herein.

Table-4. A comparison of selected values from simulated.

Amplitudes	Drop-weight Model	Acceleration (km/s^2)	Filtered acceleration (km/s^2)	Velocity (m/s)	Displacement (mm)	Strain x 10^{-2}	Stress (GPa)
1		40	4	3.	3	0.016	7.84
2		58	7.8	3	2.8	0.014	7.21
3		35	3.1	3	2.7	0.014	3.54
4		58	5.9	3.	3.2	0.014	7.12
5		52	5.2	3	2.7	0.014	3.2

A comparison of computed variables was made in Table-4 for five amplitudes. The variables' values correlate well which validated the simulation model.

Prediction of transverse shear stresses from post-processed in-plane stresses

The stresses in a laminate vary from layer to layer in stacking sequences. Image of contour plots principle strains is shown Figure-10 and in-plane normal and shear stresses of first bottom ply are shown in Figure-7 to Figure-9. If compared against ultimate strength value given Table-1 the ply is failed. However, advanced failure criteria are used to predict failure of composites which require use of transverse shear stresses.

The proposed simplified methodology of calculating transverse shear stresses returns ply-level shear stresses at any point in the panel in global *x*, *y*, *z* laminate coordinates. Three nodes (10, 92, 118) from higher concentration were selected as shown in enlarged view of Figure-6 to gather in-plane stresses for all the plies.

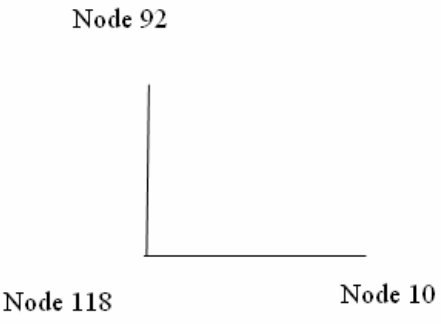

Figure-6. Schematic of enlarged view of nodes selected for through-the-thickness stresses.

Using standard numerical integration Trapezium rule and predicted in-plane stress values for through the thickness in-plane stress values were calculated as shown in Table-5 to Table-7. The calculated through-the-thickness in-plane stresses were used to calculate transverse shear stress from the standard equilibrium equations. The calculated ply by ply transverse shear stresses are given in Table-8. The expected behaviour of the transverse shear stresses is shown in Graph1 and Graph-2. These calculated transverse stresses were used in Hashin's criteria to predict failure possible modes.

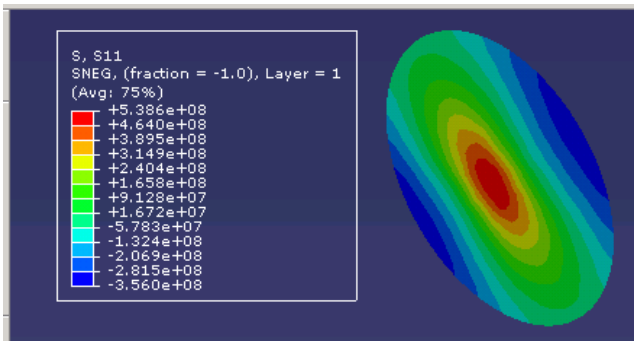

Figure-7. Contour plots of tensile stresses (σ_{11}) from 1st ply.

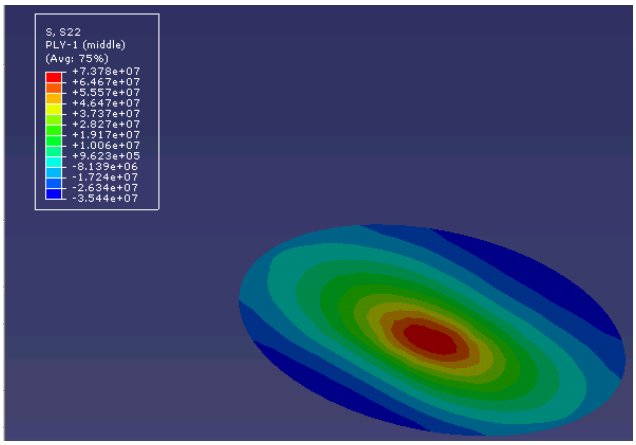

Figure-8.Contour plots of lateral stresses (σ_{11}) from 1st ply.

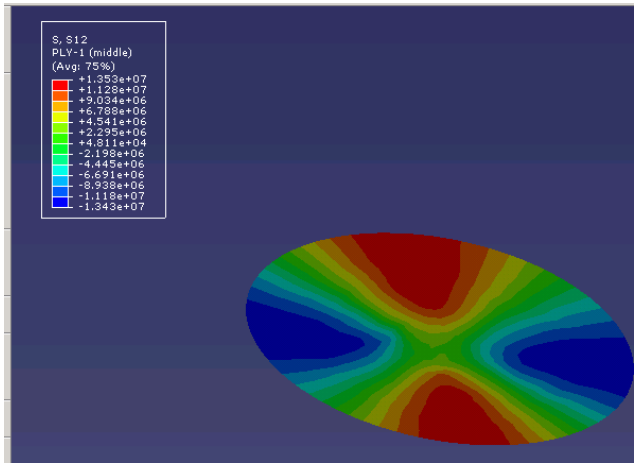

Figure-9. Contour plots of in-plane shear stresses (τ_{12}) from 1st ply.

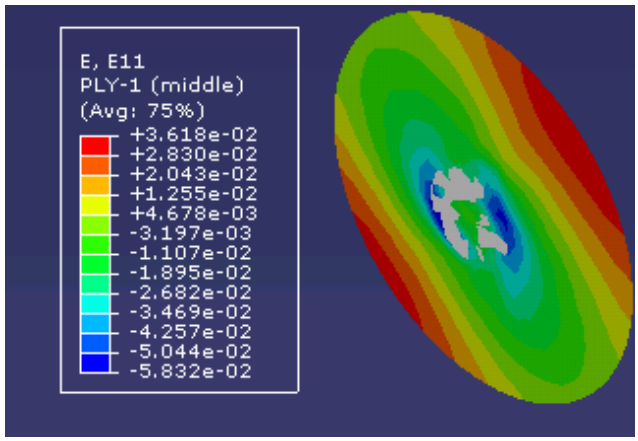

Figure-10. Contour plots of principal strains (ϵ_{11}) from 1st ply.

Tables of in-plane stress values used to calculate through-the-thickness stresses

Table-5. Predicted stresses (σ_{11}) MPa.

Ply No.	Z-dist	Node 1: 118	Node 2:10	Difference	Diff stresses	Z-dir stresses	Trapz rule
	Mm	MPa					
1	0.12	257	565	308	0.32	0.66	39.7
2	0.24	257	584	326	0.34	0.42	25.3
3	0.36	36.9	114	77.7	0.08	0.14	85.9
4	0.48	36.5	96.0	59.5	0.06	0.38	23
5	0.6	257	565	308	0.32	0.66	39.7
6	0.72	257	584	326	0.34	0.42	25.3
7	0.84	36.9	114	77.7	0.08	0.14	85.9
8	0.96	36.5	960	59.5	0.06	0.38	23
9	1.08	257	565	308	0.32	0.66	39.7
10	1.20	257	584	326	0.34	0.42	25.3
11	1.32	3.69	114	77.7	0.08	0.14	85.9
12	1.44	36.5	96.0	59.5	0.06	0.12	7.45
13	1.56	36.5	96.0	59.5	0.06	-0.02	-1.13
14	1.68	-3.69	-114.6	-77.7	-0.08	-0.42	-25.3
15	1.80	-257	-584	-326	-0.34	-0.66	-39.7
16	1.92	-257	-565	-308	-0.32	-0.38	-23
17	2.04	-36.5	-96.0	-59.5	-0.06	-0.14	-85.9
16	2.16	-36.9	-114.6	-77.7	-0.08	-0.42	-25.3
19	2.28	-257	-584	-326	-0.34	-0.66	-39.7
20	2.40	-257	-565	-308	-0.32	-0.38	-23
21	2.52	-36.5	-96.0	-59.5	-0.06	-0.14	-85.9
22	2.64	-3.69	-114	-77.7	-0.08	-0.42	-25.3
23	2.76	-257	-584	-326	-0.34	-0.66	-39.7
24	2.88	-257	-565	-308	-0.32	-0.32	-19.3

Table-6. Predicted stresses (σ_{11} and σ_{12}) MPa.

Ply No.	Z-dist	Node 1: 118	Node 2: 92	Difference	Diff stresses	Z-dir stresses	Trapz rule
	Mm	MPa					
1	0.12	23.5	29.2	5.69	0.01	0.01	0.48
2	0.24	23.4	24.2	0.781	957.00	0.00	0.09
3	0.36	60.3	60.8	0.427	523.00	0.01	0.42
4	0.48	60.4	65.7	5.33	0.01	0.01	0.81
5	0.6	23.5	29.2	5.69	0.01	0.01	0.48
6	0.72	23.4	24.2	0.781	957.00	0.00	0.09
7	0.84	60.3	60.8	0.427	523.00	0.01	0.42
8	0.96	60.4	65.7	5.33	0.01	0.01	0.81
9	1.08	23.5	29.2	5.69	0.01	0.01	0.48
10	1.20	23.4	24.2	0.781	957.00	0.00	0.09
11	1.32	60.3	60.8	0.427	523.00	0.01	0.42
12	1.44	60.4	65.7	5.33	0.01	0.01	0.78
13	1.56	60.4	65.7	5.33	0.01	0.01	0.36
14	1.68	-60.3	-60.8	-0.427	-523.00	0.00	-0.09
15	1.80	-23.4	-24.2	-0.781	-956.00	-0.01	-0.48
16	1.92	-23.5	-29.2	-5.69	-0.01	-0.01	-0.81
17	2.04	-60.4	-65.7	-5.33	-0.01	-0.01	-0.42
16	2.16	-60.3	-60.8	-0.427	-523.00	0.00	-0.09
19	2.28	-23.4	-24.2	-0.781	-956.00	-0.01	-0.48
20	2.40	-23.5	-29.2	-5.69	-0.01	-0.01	-0.81
21	2.52	-60.4	-65.7	-5.33	-0.01	-0.01	-0.42
22	2.64	-60.3	-60.8	-0.427	-523.00	0.00	-0.09
23	2.76	-23.4	-24.2	-0.781	-956.00	-0.01	-0.48
24	2.88	-23.5	-29.2	-5.69	-0.01	-0.01	-0.42

Table-7. Predicted stresses (σ_{22} and σ_{21}) MPa.

Ply No.	Z-Dist	Node 1: 118	Node 2: 10	Difference	Diff Stresses	Z-Dir Stresses	Trapz Rule
	Mm	MPa					
1	0.12	-20.4	-45.1	-24.7	-0.03	0.00	-0.21
2	0.24	20.3	41.7	2.13	0.02	0.05	2.88
3	0.36	20.4	45.1	24.7	0.03	0.00	0.21
4	0.48	-20.3	-41.7	-2.13	-0.02	-0.05	-2.88
5	0.6	-20.4	-45.1	-24.7	-0.03	0.00	-0.21
6	0.72	20.3	41.7	2.13	0.02	0.05	2.88
7	0.84	20.4	45.1	24.7	0.03	0.00	0.21
8	0.96	-20.3	-41.7	-2.13	-0.02	-0.05	-2.88
9	1.08	-20.4	-45.1	-24.7	-0.03	0.00	-0.21
10	1.20	20.3	41.7	2.13	0.02	0.05	2.88
11	1.32	20.4	45.1	24.7	0.03	0.00	0.21
12	1.44	-20.3	-41.7	-2.13	-0.02	-0.04	-2.67
13	1.56	-20.3	-41.7	-2.13	-0.02	-0.05	-2.88
14	1.68	-20.4	-45.1	-24.7	-0.03	-0.05	-2.88
15	1.80	-20.3	-41.7	-2.13	-0.02	0.00	0.21
16	1.92	20.4	45.1	24.7	0.03	0.05	2.88
17	2.04	20.3	41.7	2.13	0.02	0.00	-0.21
16	2.16	-20.4	-45.1	-24.7	-0.03	-0.05	-2.88
19	2.28	-20.3	-41.7	-2.13	-0.02	0.00	0.21
20	2.40	20.4	45.1	24.7	0.03	0.05	2.88
21	2.52	20.3	41.7	2.13	0.02	0.00	-0.21
22	2.64	-20.4	-45.1	-24.7	-0.03	-0.05	-2.88
23	2.76	-20.3	-41.7	-2.13	-0.02	0.00	0.21
24	2.88	20.4	45.1	24.7	0.03	0.03	1.54

Predicted in-plane and calculated through-the-thickness stress values

Table-8. Transverse shear stresses (MPa) calculated from Table-6 and Table-7 above.

σ_{11}	σ_{12}	σ_{13}	σ_{22}	σ_{21}	σ_{23}
MPa					
65.1	2.67	67.7	0.57	-0.43	0.14
33.9	3.09	37	0.51	0.37	0.88
31.6	-2.67	28.9	1.23	0.43	1.66
62.8	-3.09	59.7	1.28	-0.37	0.92
65.1	2.67	67.7	0.57	-0.43	0.14
33.9	3.09	37	0.51	0.37	0.88
31.6	-2.67	28.9	1.23	0.43	1.66
62.8	-3.09	59.7	1.28	-0.37	0.92
65.1	2.67	67.7	0.57	-0.43	0.14
33.9	3.09	37	0.51	0.37	0.88
16.0	-2.46	13.5	1.20	0.83	2.03
6.31	-5.56	0.75	1.14	0.46	1.60
-26.4	-5.77	-3.2.2	0.27	0.06	0.33
-65.1	-2.67	-67.7	-0.56	0.43	-0.14
-62.8	3.09	-59.7	-1.28	0.37	-0.91
-31.6	2.67	-28.9	-1.23	-0.43	-1.65
-33.9	-3.09	-37	-0.51	-0.37	-0.88
-65.1	-2.67	-67.7	-0.56	0.43	-0.14
-62.8	3.09	-59.7	-1.28	0.37	-0.92
-31.6	2.67	-28.9	-1.23	-0.43	-1.66
-33.9	-3.09	-37	-0.51	-0.37	-0.88
-65.1	-2.67	-67.7	-0.56	0.43	-0.14
-59.0	1.75	-57.3	-0.89	0.59	-0.31
-19.3	1.54	-17.7	-0.24	0.19	-0.05

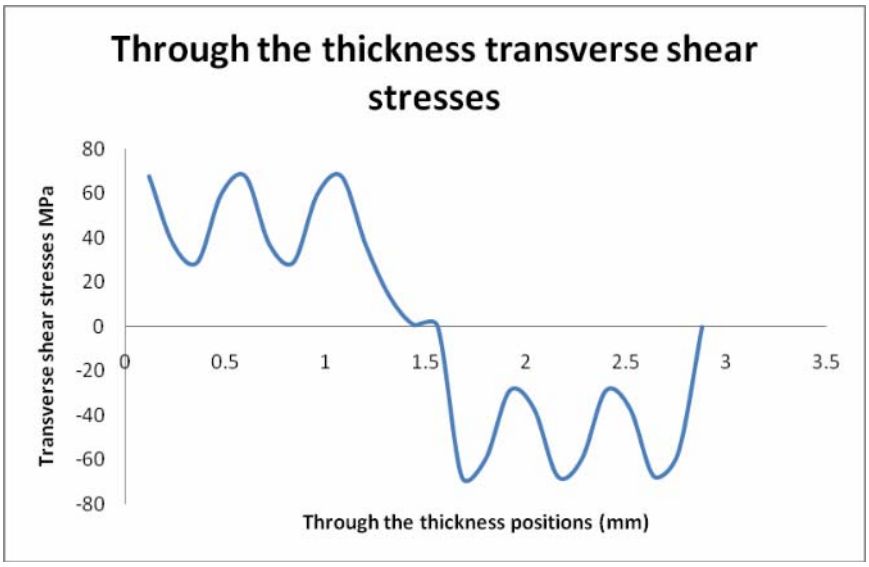

Graph-1. Transverse shear stresses σxz MPa versus thickness (mm).

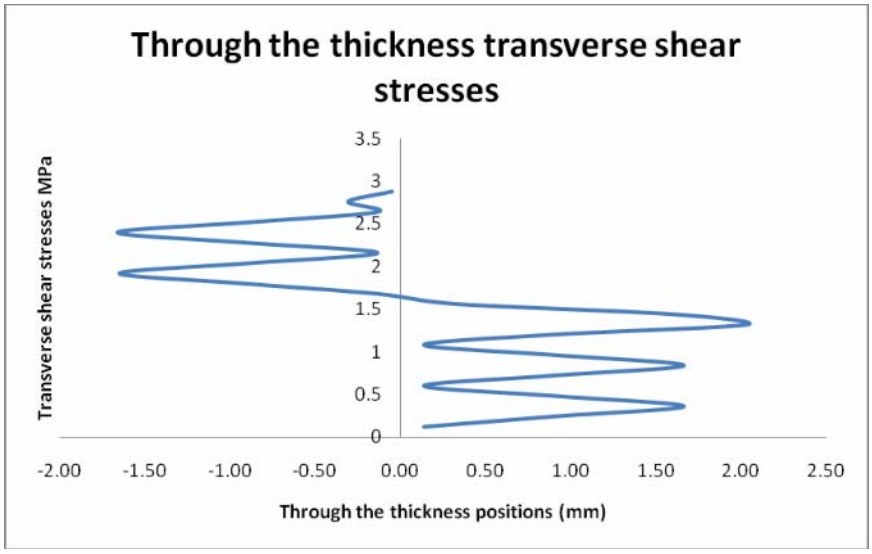

Graph-2. Transverse shear stresses σ_{yz} MPa versus thickness positions (mm).

Failure prediction using Hashin's failure criteria

Computed values of the principal stresses and strains were compared with the allowable stresses against the given values and Maximum Stress and Maximum Strain failure criteria. The shortcoming of such conventional failure theories including Tsai-Hill and Tsai-Wu criteria are that they do not explicitly differentiate matrix failure from fibre failure. Hashin developed a set of interactive failure criteria in which distinct failure modes are modelled. The failure modes included in Hashin's criteria are as follows.

Tensile fibre failure for $\sigma_{11} \geq 0$

$$\left(\frac{\sigma_{11}}{X_T}\right)^2 + \frac{\sigma_{12}^2 + \sigma_{13}^2}{S_{12}^2} = \begin{cases} \geq 1 & \text{failure} \\ < 1 & \text{no failure} \end{cases} \quad (1)$$

Compressive fibre failure for $\sigma_{11} < 0$

$$\left(\frac{\sigma_{11}}{X_C}\right)^2 = \begin{cases} \geq 1 & \text{failure} \\ < 1 & \text{no failure} \end{cases} \quad (2)$$

Tensile matrix failure for $\sigma_{22} + \sigma_{33} > 0$

$$\frac{(\sigma_{22} + \sigma_{33})^2}{Y_T^2} + \frac{\sigma_{23}^2 - \sigma_{22}\sigma_{33}}{S_{23}^2} + \frac{\sigma_{12}^2 + \sigma_{13}^2}{S_{12}^2} = \begin{cases} > 1 & \text{failure} \\ \leq 1 & \text{no failure} \end{cases} \quad (3)$$

Where σ_{ij} denote the stress components and the tensile and compressive allowable strengths for lamina are denoted by subscripts *T* and *C*, respectively. X_T, Y_T, Z_T denotes the allowable tensile strengths in three respective material directions. Similarly, X_C, Y_C, Z_C denotes the allowable tensile strengths in three respective material directions. Further, S_{12}, S_{13} and S_{23} denote allowable shear strengths in the respective principal material directions. When calculated transverse shear stresses used in Eq. (1) to Eq. (3) expected delamination failure modes were achieved. The prediction considering the transverse shear stresses matched and agreed well. If the load is increased further the damaged areas further increase as well as lead to de-lamination growth and failure.

CONCLUSIONS

Efficient and reliable computation methodology of drop-weight impact on fibre reinforced composite was implemented in the commercially available software ABAQUS™. Transverse shear stresses were predicted from post-processing in-plane stresses without 3-D analysis. The predicted stresses were used to predict failure for various configurations and their results were compared. To improve convergence, adaptive meshing techniques were employed to mesh the regions of high stress gradient with fine meshes. The predicted results were found within ±10% of the strains and displacements of those obtained from experimental values measured by (James, 2006). Failure prediction using from the models means that the simulation models are adequate and reliable.

The analysis can be modified easily if ply configurations, orientations, or the laminate differs in properties and thickness. To incorporate such changes the effected plies need to be changed. If damage or various material properties and geometrical conditions need to be introduced, the effective number of plies can be easily replaced.

REFERENCES

J.K. Chen and C.T. Sun. 1985. Dynamic large deflection response of composite laminates subjected to impact. Compos Struct. 4: 59-73.

S. Abrate. 1991. Impact on laminated composites. Appl Mech Rev. 44(4): 155-190.
H.Y. Choi and F.K. Chang. 1991. A new approach toward understanding damage mechanisms and mechanics of laminated composites due to low velocity impact loading. J. Compos. Mater. (Part I and II). 25: 992-1038.

H.Y. Choi and F.K. Chang. 1992. A model for predicting damage in graphite/epoxy composites resulting from low-velocity point impact. J Compos Mater. 26: 2134-2169.

I.H. Choi and C.S. Hong. 1994. Low-velocity impact response of composites considering higher-order shear deformation and large deflection. Mech Com Mater Struct. 1: 157-170.

Choi IH. 1994. Response and damage of composite laminates subjected to low-velocity impact. The PhD Thesis, Korea Advanced Institute of Science and Technology.

Hong CS, Choi IH, Kim CG. 1994. Estimation of damage area due to low-velocity impact in composite laminate. In: 9th Technical conference proceeding of the American Society for Composites. pp. 473-81.

M.D. Robb, W.S. Arnold and I.H. Marshall. 1995. The damage tolerance of GRP laminates under biaxial prestress. Compos Struct. 32: 141-149.

Pierson M.O. and Vaziri R. 1995. Analytical solution for low-velocity impact response of composites. AIAA J. 34: 1633-1640.

Sekine H., Hu N., Fukunaga H. and Natsume. 1998. T. Low-velocity impact response of composite. Mech Compos Mater Struct. 5: 275-278.

S. Ganapathy and K.P. Rao. 1998. Failure analysis of laminated composite cylindrical/spherical shell panels subjected low velocity impact. Comput. Struct. 68: 627-641.

Mili F. and Necib B. 2001. Impact behavior of cross-ply composites under low velocities. Compos Struct. 51: 237-244.

S. Abrate. 2001. Modeling of impacts on composite structures. Compos Struct. 51(2): 129-138.

Li C.F., Hu N., Yin Y.J., Sekine H. and Fukunaga H. 2002. Low-velocity impact damage of composites. Part I An FEM model. Comp. pp. 1055-1062.

Aslan Z., Karakuza R. and Okutan B. 2003. The response of composites under low-velocity impact. Compos Struct. 59: 119-127.

B. Whittingham, I.H. Marshall, T. Mitrevski and R. Jones. 2004. The response of composites with pre-stress subject to low velocity impact damage. Compos Struct. 66: 685-698.

ABAQUS Users' Manual, Version 6.6, ©2006 ABAQUS, Inc.

James R. A. 2006. Impact Damage Resistance and Damage Tolerance of Fibrous Composites. PhD Thesis. University of Bolton, UK.

T. Mitrevski, I.H. Marshall, R.S. Thomson and R. Jones. 2006. Low-velocity impacts on preloaded GFRP specimens with various impactor shapes. Compos Struct. 76: 209-217.

R. Tiberkak, M. Bachene, S. Rechak and B. Necib. 2008. Damage prediction in composite plates subjected to low velocity impact. Compos Struct. 83: 73-82.

Farooq U. and Gregory K. 2009. Computational modeling and simulation of low velocity impact on composite panels un-partitioned model. ARPN Journal of Engineering and Applied Sciences. 4(2).